ACS APPLIED NANO MATERIALS

www.acsanm.org Article

# Dual-Shaped Silver Nanoparticle Labels for Electrochemical Detection of Bioassays

Nicole E. Pollok, Yi Peng, Nikhil Raj, Charuksha Walgama, and Richard M. Crooks*

Cite This: *ACS Appl. Nano Mater.* 2021, 4, 10764−10770 Read Online

ACCESS | Metrics & More | Article Recommendations | Supporting Information

**ABSTRACT:** In this paper, we demonstrate the use of dual-shaped silver nanoparticles (AgNPs) as detection labels for electrochemical bioassays. The key finding is that by simultaneously using AgNP labels having two different shapes, the limit of detection (LOD) for the assays is lowered compared to using either of the two shapes separately. The two shapes were silver nanocubes (AgNCs) having edge lengths of 40 ± 4 nm and spherical AgNPs (sAgNPs) having diameters of 20 ± 3 nm. Two different bioassays were examined. In both cases, the Ag labels were functionalized with antibodies. In the first assay, the labels are directly linked to a second antibody immobilized on magnetic beads. In the second assay, the antibodies on the AgNP labels and the antibodies on the magnetic beads are linked via a peptide. The peptide is N-terminal prohormone brain natriuretic peptide (NT-proBNP), which is a heart-failure marker. The efficacy of the two electrochemical assays as a function of the ratio of the two labels was investigated using a galvanic exchange/anodic stripping voltammetry method. The key finding is that by optimizing the ratio of the two types of AgNP labels, it is possible to decrease the LOD of the assays without compromising the dynamic range compared to using either of the two labels independently. This made it possible to achieve the clinically relevant range for NT-proBNP analysis used by physicians for heart failure risk stratification.

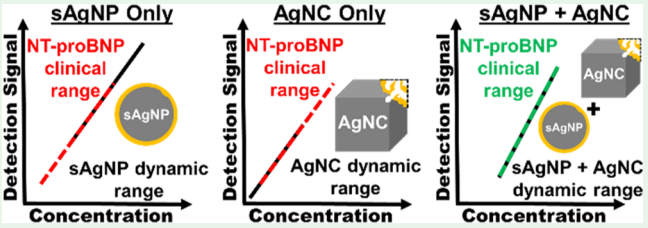


**KEYWORDS:** *spherical silver nanoparticles, silver nanocubes, metalloimmunoassay, galvanic exchange, N-terminal prohormone brain natriuretic peptide, heart failure*



## INTRODUCTION

Here, we report on the simultaneous use of two different Ag nanoparticle (NP) shapes as detection labels for electrochemical bioassay signal amplification. The two shapes, nanocubes (AgNCs) and spherical NPs (sAgNPs), are responsive to different concentration ranges of the assay. Accordingly, the novelty of this work is that by combining the two shapes into a single assay, the dynamic range is expanded compared to using either of the two shapes individually. Specifically, both NPs were functionalized with a monoclonal antibody and tethered to a magnetic microbead (M$\mu$B) surface prior to electrochemical detection. Using a previously reported galvanic exchange and anodic stripping voltammetry (GE/ASV) detection method,[1] the optimal ratio of these particles on the M$\mu$B surface was systematically investigated.

Compared to a single label, the simultaneous use of both the sAgNP and AgNC labels leads to the following results. First, there is a threefold decrease in the limit of detection (LOD) for a model immunoassay. Second, the total amount of Ag charge collected increases by 20%. Third, the LOD for a metalloimmunoassay for the heart-failure biomarker N-terminal prohormone brain natriuretic peptide (NT-proBNP) decreases by an order of magnitude. This decrease results in the metalloimmunoassay overlapping with the clinically relevant concentration range and risk stratification threshold for NT-proBNP.[2−5] This latter goal could not be achieved using either of the two AgNP shapes individually.[6]

NPs differing in composition,[7,8] size,[9] shape,[10] and surface modifications[11−13] have been applied to a variety of assays and bioassays.[6,14,15] Due to their robust characteristics, the optical,[16−19] magnetic,[20] and electrochemical[6,11,14,21,22] properties of metal NPs have been utilized for immunological assays in the biosensor field in place of the more common enzymatic,[23,24] fluorescent,[25] and radioactive[26] labels.[27,28] Gold NPs are the most commonly used metallic labels for bioassays, primarily due to their stability and their desirable optical properties.[29−32] Although AgNPs also have useful optical properties, they are significantly less stable than AuNPs.[33] This is a consequence, in part, of the fact that Ag has a much lower standard potential ($E^\circ$ = 0.79 V) than Au ($E^\circ$ = 1.52 V).[34] For many applications, this large difference in standard potentials is a drawback, but as we have shown previously, it can also be an advantage.[1,14,33]

**Received:** July 29, 2021
**Accepted:** September 29, 2021
**Published:** October 13, 2021

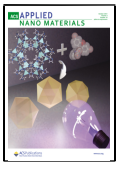




https://doi.org/10.1021/acsanm.1c02207
*ACS Appl. Nano Mater.* 2021, 4, 10764−10770

Our group has previously combined GE with ASV to detect the heart failure marker NT-proBNP using sAgNPs.[6,14] Scheme 1a–c illustrates how sAgNP labels are detected in

**Scheme 1. Schematic Illustration of the Galvanic Exchange/Anodic Stripping Voltammetry (GE/ASV) Detection Method Involving (a–c) sAgNPs or (d–f) AgNCs**

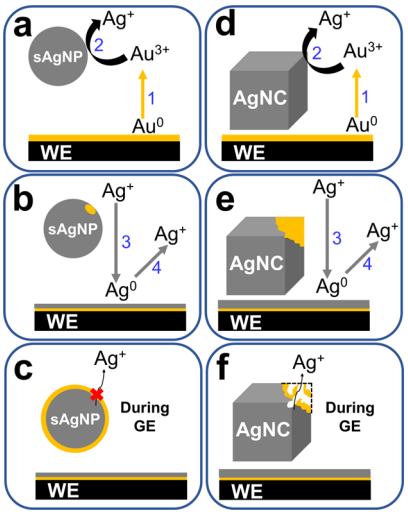


these studies. As shown in Scheme 1a, metallic Au predeposited on the detection working electrode (WE) is first oxidized. The resulting $Au^{3+}$ (here representing all species of oxidized Au) diffuses into the sAgNPs and partially oxidizes them to $Ag^+$ by GE. Next, as shown in Scheme 1b, the resulting $Ag^+$ is electrodeposited onto the surface of the WE. This can be thought of as a preconcentration step. Finally, the surface-bound Ag is electrochemically oxidized by ASV. The charge resulting from the ASV step corresponds to the detection signal. The GE step is essential in this approach because the distance between the sAgNP labels (which are linked to the ~1.0 $\mu$m-diameter M$\mu$Bs) and the WE precludes direct oxidation of the sAgNPs. An intrinsic drawback of the GE process is that, depending on their size, a Au shell may form around the sAgNPs, thereby preventing complete oxidation (Scheme 1c).[35,36]

In an effort to circumvent the foregoing partial sAgNP oxidation problem and thereby lower the LOD for GE/ASV assays, we recently introduced the idea of replacing sAgNPs with AgNC labels.[37] AgNCs are known to form a more porous Au shell during GE with $Au^{3+}$ (Scheme 1d–f),[38−42] and we reasoned that this would result in a higher ASV charge and thus a lower LOD for the NT-proBNP assay. Scheme 1c–f illustrates the general conclusions from these earlier reports as they relate to the present study. Comparison of Scheme 1c,f illustrates the key point: GE is prematurely terminated by the formation of the Au shell in Scheme 1c, but the porous Au shell of the AgNCs (Scheme 1f) permits more complete GE.[37,39−43]

In this article, a combination of AgNC and sAgNP labels was used to detect both a model assay and an antigen-specific assay for NT-proBNP. In Scheme 2, the formation of the metalloimmunoassay for the detection of NT-proBNP is depicted. This metalloimmunoassay is formed by first capturing the analyte of interest from solution on a M$\mu$B and then completing the immunosandwich with the functionalized AgNCs and sAgNPs. In the second step of assay

**Scheme 2. Schematic Illustration of the Formation of the Metalloimmunoassay Using Both the sAgNP-Ab and AgNC-Ab Bioconjugates in the Presence of the Biomarker**

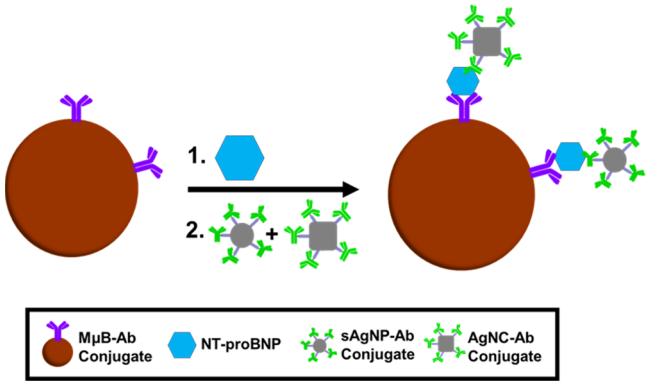


formation, the two differently shaped Ag labels are shown. The main difference between the current work and our previously reported AgNC investigation is the application of this AgNC label to a biomarker-containing metalloimmunoassay and the use of the AgNC labels in conjunction with the sAgNP labels within the same assay.

As alluded to earlier, previous results from our laboratory showed that sAgNP labels yield a broad dynamic range but an insufficient lower LOD for this assay.[6,14] Conversely, AgNC labels result in a limited dynamic range but a superior LOD. Accordingly, we hypothesized that by combining the two types of NPs it would be possible to access the clinically relevant range for NT-proBNP detection.[2−5] The key point is that this hypothesis is proven correct by the results presented herein.

## EXPERIMENTAL SECTION

**Chemicals and Materials.** Information about the chemicals and materials is provided in the Supporting Information.

**Electrochemistry.** The electrochemical measurements have been described previously.[1,6,14,33]

**Preparation of the Conjugates.** Information about the Ag-Ab and M$\mu$B-Ab conjugates and formation of the NT-proBNP assay has been described previously.[37,44]

**Preparation of the M$\mu$B-Ab Conjugates.** For the model assay, the biotinylated SAb was conjugated to streptavidin-coated M$\mu$Bs using the protocol provided by the manufacturer.[45] Specifically, 100 $\mu$L of M$\mu$Bs (~7–10 × $10^9$ M$\mu$Bs/mL) was aliquoted and washed. Washing was performed using magnetic separation, wherein the M$\mu$Bs were collected on the wall of an SBB-blocked microcentrifuge tube with a neodymium magnet, the supernatant was removed, and the conjugate was redispersed in phosphate-buffered saline (PBS). This process was carried out three times. Next, 40.0 $\mu$L of 6.67 $\mu$M SAb was added to the tube, and the resulting solution was incubated for 30 min at 40 rpm at RT using the tube revolver. Finally, the conjugated M$\mu$Bs were washed using magnetic separation five times with 100 $\mu$L of SBB and then redispersed in a final volume of 100 $\mu$L of SBB. The resulting conjugate is referred to as M$\mu$B-SAb.

For the NT-proBNP assay, the 15C4 capture Ab was biotinylated using a kit and the protocol provided by the manufacturer.[46] Next, the modified Ab was conjugated to the streptavidin-coated M$\mu$Bs using the same procedure as described for the M$\mu$B-SAb, wherein 40.0 $\mu$L of the 6.67 $\mu$M biotinylated 15C4 capture Ab was incubated with 100 $\mu$L of the streptavidin-coated M$\mu$Bs for 1 h at 30 rpm at RT on the tube revolver. After incubation, the conjugate was washed by magnetic separation. The resulting product is referred to as the M$\mu$B-15C4 conjugate.


https://doi.org/10.1021/acsanm.1c02207
ACS Appl. Nano Mater. 2021, 4, 10764−10770

**Formation of the Metalloimmunoassays.** Information about the formation of the metalloimmunoassays is provided in the Supporting Information.

## RESULTS AND DISCUSSION

**Electrochemical Analysis of the sAgNP-Ab and AgNC-Ab Conjugates.** The first step for comparing the efficacy of the sAgNP-Ab and AgNC-Ab conjugates was to determine a figure of merit that could remain constant for both of them. These two types of NPs are similar in that they are both composed of Ag and they both have HBCL-modified Abs bioconjugated to their surface. There are, however, some differences. Specifically, these NPs differ in size (20 vs 40 nm diameter for sAgNPs and AgNCs, respectively), surface ligands (poly(ethylene glycol) vs poly(vinylpyridine) for sAgNPs and AgNCs, respectively), and GE efficiency. Accordingly, the best figure of merit is the total Ag charge collected after the GE/ASV detection method is performed on the model composites. Briefly, the M$\mu$B-sAgNP and M$\mu$B-AgNC model composites were prepared as described in the Experimental Section using different concentrations of just the sAgNP-Ab or just the AgNC-Ab conjugates. These formed composites were then transferred to the paper-electrode platform for electrochemical analysis. The goal for this first experiment was to determine a concentration of both composites that would lead to the same amount of charge collected by GE/ASV. The results would then provide a context for comparing the labels in subsequent experiments.

Figure 1 is a histogram comparing the Ag charge obtained using 100 pM of just the M$\mu$B-sAgNP model composite or 60.8 pM of just the M$\mu$B-AgNC model composite. The results indicate that at these concentrations, there is no statistical difference in the charge collected using the two different model composites. Specifically, both model composites, which were prepared with Ag particles having different sizes, shapes, and surface ligands, resulted in a Ag charge of ~25.0 $\mu$C.

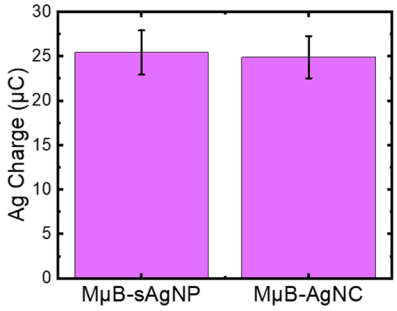


**Figure 1.** Histograms representing the amount of Ag charge obtained by forming the model composite assay with either sAgNP-Ab or AgNC-Ab conjugates (100 and 60.8 pM, respectively). These model composites were prepared using the M$\mu$B-SAb conjugate and either only the sAgNP-Ab conjugate, to make the "M$\mu$B-sAgNP" model composite, or only the AgNC-Ab conjugate, to make the "M$\mu$B-AgNC" model composite. Following assay formation, the samples were both washed and aliquoted, as described in the Experimental Section, and transferred to the paper electrode for analysis in 50.0 $\mu$L of PBS. The error bars represent the standard deviation from the mean for five independent measurements.

**Optimization of the NP Ratio.** After establishing an appropriate context for comparing the sAgNP-Ab and AgNC-Ab conjugates (Figure 1), the model composite was systematically prepared using mixtures of the sAgNP-Ab and AgNC-Ab conjugates. The different volumetric ratios of the two conjugates were prepared using a 100 pM solution of the M$\mu$B-sAgNP model composite and a 60.8 pM solution of the M$\mu$B-AgNC model composite. These solutions were prepared as described in the Experimental Section and summarized in Table S1. The key point is that the concentrations of the two composites (100 or 60.8 pM) used individually yield the same detection signal (Figure 1). Henceforth, we refer to this as "Ag charge equivalence". Therefore, when the two labels are mixed in different ratios, it is possible to determine if a particular ratio leads to an optimal dynamic range and LOD that are superior to those when either of the two labels used individually.

The histograms in Figure 2a correspond to the Ag charge collected when the model composite was formed with volume

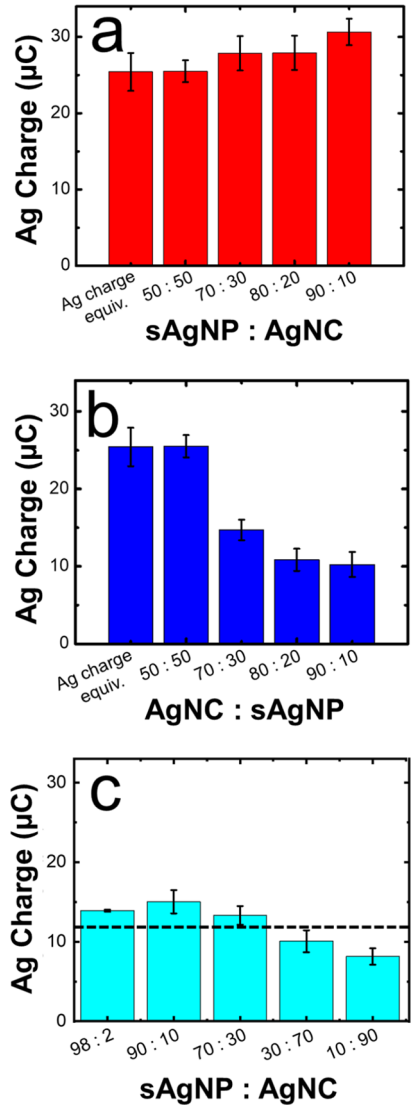


**Figure 2.** Histograms representing the amount of Ag charge collected from the model composite when it was prepared using different volumetric ratios of 100 pM sAgNP-Ab and 60.8 pM AgNC-Ab conjugates (Table S1). (a) NP ratios containing more sAgNPs than AgNCs (sAgNP/AgNC) and (b) NP ratios containing more AgNCs than sAgNPs (AgNC/sAgNP). (c) Same experiment as in (a) but the concentration of the model composite was diluted by 50%. The dashed line represents the expected Ag charge based on the result for the "Ag charge equivalence" in (a). The error bars represent the standard deviation from the mean for five independent measurements.



https://doi.org/10.1021/acsanm.1c02207
ACS Appl. Nano Mater. 2021, 4, 10764−10770

ratios that included more sAgNPs than AgNCs in the mixture. For example, for the 70:30 model composite, 70.0 $\mu$L of the sAgNP-Ab conjugate and 30.0 $\mu$L of the AgNC-Ab conjugates were added to 16.0 $\mu$L of M$\mu$B-SAb (Table S1). The Ag charge corresponding to this and other ratios is compared to the "Ag charge equivalence" (first histogram in Figure 2a). Recall, that the Ag charge equivalence is the Ag charge resulting from the model composite yielding the same Ag charge but comprising only sAgNPs or only AgNCs (Figure 1). The results in Figure 2a show that the 90:10 NP ratio generated a Ag charge which was ~20% higher than when the model composite is formed with only the sAgNPs or only the AgNCs.

The histograms in Figure 2b were obtained exactly as discussed for Figure 2a, except for NP ratios that included more AgNCs than sAgNPs. The results indicate that when there are more AgNCs than sAgNPs present in the labeling mixture, the Ag charge collected after the GE/ASV detection method is significantly lower than the Ag charge equivalence results. The results in Figure 2b indicate that NP ratios that include more AgNCs than sAgNPs are not optimal for sensing applications.

Up to this point, a relatively high concentration of the sAgNPs-Ab and AgNC-Ab conjugates (various percentages having concentrations of 100 and 60.8 pM, respectively) was used to form the model composite. The next step in the optimization process was to reduce the NP concentration by 50% (Figure 2c) to ensure that the same trends are observed over a range of concentrations (as would be encountered in a bioassay). An additional 98:2 ratio was also included in this part of the study. The dotted line in Figure 2c represents the expected Ag charge if the initial Ag concentration was diluted by 50%. That is, the benchmark value used in this experiment was the Ag charge equivalence, which resulted in ~25.0 $\mu$C of charge (Figure 1). Therefore, the expected Ag charge when the concentration is reduced by 50% is ~12.5 $\mu$C. The data in Figure 2c show that even when the concentration is reduced, the 90:10 sAgNP/AgNC ratio still results in a 20% increase in the expected Ag charge. On the basis of these results, the 90:10 sAgNP/AgNC ratio was used for the remaining experiments.

**Calibration Curve for the 90:10 sAgNP/AgNC Model Composite.** After confirming that the 90:10 sAgNP/AgNC ratio is optimal for one concentration of Ag, this same ratio was applied to a series of different Ag concentrations. Accordingly, the model composite was prepared as described in the Experimental Section using a 90:10 volumetric ratio of the sAgNP-Ab and AgNC-Ab conjugates at total Ag NP concentrations ranging from 2.07 to 100 pM. The formed model composites were then washed using magnetic separation and transferred to the paper-electrode for electrochemical analysis.

Figure 3 shows the results of this experiment. Specifically, the representative voltammograms in Figure 3a indicate that the Ag oxidation current increases as a function of the total concentration of AgNPs used to form the model composite assay. The inset includes an expanded view of the voltammogram for the blank (black trace). This solution contained AgNPs that were not bioconjugated to Abs, and it demonstrates that the assay has an intrinsic zero background. The inset also shows data for the lowest detectable AgNP concentration (2.07 pM, red trace).

The charges under voltammograms like those shown in Figure 3a, plus voltammograms obtained at other concentrations (Figure S2), were obtained by integration, and the results for five independent experiments per concentration are plotted in Figure 3b. These data demonstrate that the charge increases linearly from 2.07 to 100.0 pM of total AgNPs (sAgNPs + AgNCs) and then begins to saturate. Note that concentrations below 2.07 pM could not be differentiated from the blank and thus are not shown in Figure 3. Nevertheless, the LOD of 2.07 pM represents a threefold decrease compared to the same assay carried out using only sAgNPs (Figure S1). Another important aspect of Figure 3b is that the relative standard deviation of the combined dataset is <11%.

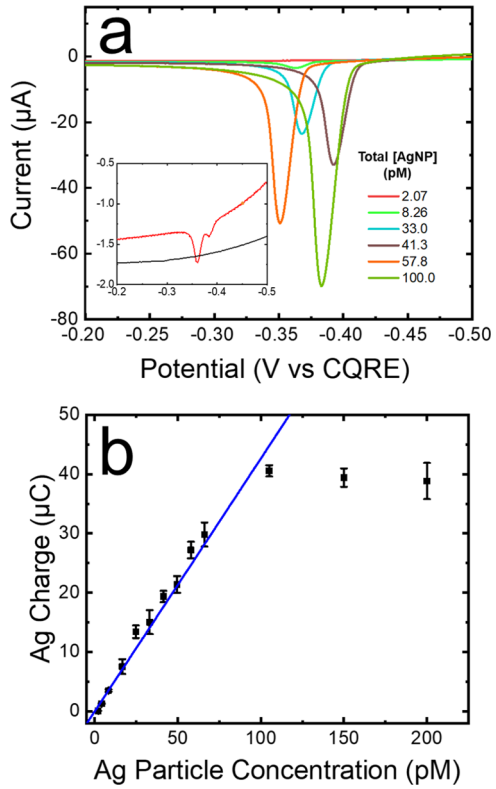


**Figure 3.** Electrochemical results for detection of the model composite formed using the 90:10 sAgNP/AgNC volumetric ratio and the GE/ASV detection protocol. (a) Representative ASV curves for the total concentration of AgNPs (sAgNPs + AgNCs) indicated in the legend. The inset includes an expanded view of the voltammogram for the blank (black trace). For clarity, representative ASV curves for only half of the concentrations used to construct the calibration curve in (b) are shown. The other half are provided in Figure S2. The position of the ASV peaks varies somewhat because the references electrode is a CQRE. (b) Calibration curve showing the correlation between the Ag charge [obtained by integrating ASV curves like those in (a)] and the total AgNP concentrations (sAgNPs + AgNCs). This plot contains data shown in (a) and in Figure S2. The LOD, 2.07 pM, was calculated using the standard deviation of the linear regression line and the slope of the calibration curve. The linear regression value is 0.99 and the scan rate was 50 mV/s. Each data point represents the average of five measurements carried out using independently fabricated electrodes. The error bars represent the standard deviation of these five measurements. Outliers were eliminated using Grubb's test with a 95% confidence level.

**Dose–Response Curve for the NT-proBNP Metalloimmunoassay.** The ultimate goal in this dual-shaped AgNP investigation is to ensure that the results leading up to this point can be translated to the NT-proBNP metalloimmunoassay, which is the main focus of our sensor-related research.


https://doi.org/10.1021/acsanm.1c02207
ACS Appl. Nano Mater. 2021, 4, 10764−10770

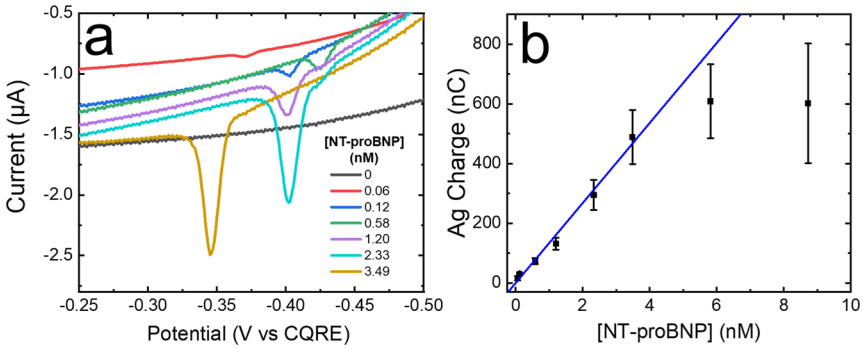


**Figure 4.** Electrochemical results obtained for detection of NT-proBNP using the 90:10 sAgNP/AgNC volumetric ratio and the GE/ASV detection protocol. (a) Anodic stripping voltammograms were obtained by aliquoting 2.0 μL of the formed assay, diluting it with 48.0 μL of PBS, and then carrying out the GE/ASV protocol described in the text. The concentrations listed in the legend represent the concentrations of NT-proBNP used to form the metalloimmunoassay. The scan rate was 50 mV/s. (b) Calibration curve showing the correlation between the Ag charge [obtained by integrating ASV curves like those in (a)] and the concentration of NT-proBNP used to form the immuno-sandwich. Additionally, for clarity, the ASV curve for 5.82 nM of NT-proBNP is not shown in Figure 4a. The error bars represent the standard deviation obtained using five independent measurements. Outliers were eliminated using Grubb's test with a 95% confidence level.

Accordingly, the NT-proBNP bioassay was prepared in SuperBlock Blocking buffer (SBB) using the step-wise procedure described in the Experimental Section. Specifically, 16.0 μL of the MμB-15C4 conjugate was added to SBB-blocked microcentrifuge tubes, and then, 100 μL of different concentrations of NT-proBNP was added. The control for this experiment was the formation of the metalloimmunoassay in the absence of NT-proBNP. Following incubation and washing, an excess of the 90:10 sAgNP/AgNC conjugate ratio was added to the tubes. The fully formed assay was then transferred to the paper electrode, and the electrochemical detection protocol was carried out in PBS.

Representative ASV curves for this experiment are shown in Figure 4. The voltammograms in Figure 4a indicate that the Ag stripping current increases as a function of the concentration of the NT-proBNP used to form the assay. Note, however, that concentrations below 0.06 nM could not be differentiated from the background. The charges under voltammograms like those shown in Figure 4a were obtained by integration, and the results for five independent experiments per concentration are plotted in Figure 4b. These data show that the linear dynamic range for this assay is 0.06−3.49 nM of NT-proBNP and that at higher concentrations, the calibration curve begins to saturate. The average relative standard deviation for the points on the linear part of the calibration curve is <21%.

Earlier we stated that the lowest LOD we have been able to achieve for the NT-proBNP metalloimmunoassay formed using only the sAgNP-Ab conjugate was about fivefold higher than the clinically relevant minimum value. Specifically, the lowest LOD heretofore achieved was 0.58 nM,[6] but the minimum clinical concentration used by physicians to identify heart failure patients who are at risk of poor outcomes is 0.116 nM.[2−5] Using the dual-shaped AgNP conjugates, the limit of detection for this bioassay is 0.06 nM, well below the target of 0.116 nM. We attribute this lower LOD to the incorporation of the AgNC-Ab conjugates into the Ag detection labels used in this bioassay. Recall that according to previously published literature, the AgNCs perform more efficiently during the GE process than the sAgNPs because the Au shell formed around the AgNCs is more porous, and therefore, more exchange can occur.[37,39−43]

## SUMMARY AND CONCLUSIONS

The overall goal of the present article was to develop an assay for the heart failure biomarker NT-proBNP that could perform within the clinically relevant concentration range. This range includes the risk stratification threshold used by physicians to determine next steps in the care of a patient. We have previously reported on this specific assay in which only sAgNPs were used as detection labels.[6] The use of only the sAgNP labels resulted in an LOD which was still fivefold higher than the clinically relevant minimum concentration of NT-proBNP. In an effort to reduce the LOD of the assay, AgNCs were introduced as an additional detection label. This decision was made because prior literature indicated that AgNCs experience more efficient GE with $Au^{3+}$ than sAgNPs.[37,39−43] Specifically, instead of a Au shell forming around the exterior of the NPs, as occurs for sAgNPs,[35,36] a porous Au layer forms. The porous Au layer results in more exchange during the GE process.[37,39−43]

The optimal volumetric ratio of the two labels was found to be 90:10 sAgNP/AgNCs. Using both types of labels simultaneously, we achieved a threefold decrease in the LOD for the model metalloimmunoassay. We attribute this result to the presence of the AgNCs, which undergo more efficient GE than the sAgNPs. The findings for the model assay translated well to the antigen-specific assay for NT-proBNP. In particular, the LOD for the metalloimmunoassay for NT-proBNP decreased by an order of magnitude, but the high end of the dynamic range was not affected by the presence of the AgNCs.[6] Accordingly, the NT-proBNP assay overlaps with the clinically relevant concentration range and risk stratification threshold for NT-proBNP in buffer.[2−5] The next steps for this NT-proBNP assay include transitioning it into a serum matrix with the dual-shaped AgNP detection labels. The results of this work will be reported in due course.

## ASSOCIATED CONTENT

### Supporting Information

The Supporting Information is available free of charge at https://pubs.acs.org/doi/10.1021/acsanm.1c02207.

Chemicals and materials; procedure for the fabrication of the paperelectrodes; sAgNP-Ab and AgNC-Ab ratios used for forming the model and NT-proBNP assays;



https://doi.org/10.1021/acsanm.1c02207
ACS Appl. Nano Mater. 2021, 4, 10764−10770

procedure for the synthesis of the AgNCs; formation of the metalloimmunoassays; calibration curve for the model composite formed using only the sAgNP-Ab conjugate; and selected ASV traces (PDF)

## AUTHOR INFORMATION


### Corresponding Author

**Richard M. Crooks** − *Department of Chemistry, The University of Texas at Austin, Austin, Texas 78712-1224, United States;* orcid.org/0000-0001-5186-4878; Email: crooks@cm.utexas.edu

### Authors

**Nicole E. Pollok** − *Department of Chemistry, The University of Texas at Austin, Austin, Texas 78712-1224, United States*

**Yi Peng** − *Department of Chemistry, The University of Texas at Austin, Austin, Texas 78712-1224, United States;* orcid.org/0000-0002-5319-1336

**Nikhil Raj** − *Department of Chemistry, The University of Texas at Austin, Austin, Texas 78712-1224, United States*

**Charuksha Walgama** − *Department of Chemistry, The University of Texas at Austin, Austin, Texas 78712-1224, United States;* Present Address: Department of Physical & Applied Sciences, University of Houston-Clear Lake, 2700 Bay Area Boulevard, Houston, TX 77058, USA

Complete contact information is available at: https://pubs.acs.org/10.1021/acsanm.1c02207


### Notes

The authors declare the following competing financial interest(s): The technology reported in this manuscript could eventually be used by Galvanyx, LLC. The corresponding author has an interest in this company.

## ACKNOWLEDGMENTS

Research reported in this publication was supported by the National Heart, Lung, and Blood Institute of the National Institutes of Health under award R01HL137601. The content is solely the responsibility of the authors and does not necessarily represent the official views of the National Institutes of Health. We also thank the Robert A. Welch Foundation (grant F-0032) for sustained support of our research.

## REFERENCES


(1) Kogan, M. R.; Pollok, N. E.; Crooks, R. M. Detection of Silver Nanoparticles by Electrochemically Activated Galvanic Exchange. *Langmuir* **2018**, *34*, 15719−15726.

(2) Zile, M. R.; Claggett, B. L.; Prescott, M. F.; McMurray, J. J. V.; Packer, M.; Rouleau, J. L.; Swedberg, K.; Desai, A. S.; Gong, J.; Shi, V. C.; Solomon, S. D. Prognostic Implications of Changes in N-Terminal Pro-B-Type Natriuretic Peptide in Patients With Heart Failure. *J. Am. Coll. Cardiol.* **2016**, *68*, 2425−2436.

(3) Felker, G. M.; Ahmad, T.; Anstrom, K. J.; Adams, K. F.; Cooper, L. S.; Ezekowitz, J. A.; Fiuzat, M.; Houston-Miller, N.; Januzzi, J. L.; Leifer, E. S.; Mark, D. B.; Desvigne-Nickens, P.; Paynter, G.; Piña, I. L.; Whellan, D. J.; O'Connor, C. M. Rationale and Design of the Guide-It Study: Guiding Evidence Based Therapy Usingbiomarker Intensified Treatment in Heart Failure. *JACC Hear. Fail.* **2014**, *2*, 457−465.

(4) Masson, S.; Latini, R.; Anand, I. S.; Vago, T.; Angelici, L.; Barlera, S.; Missov, E. D.; Clerico, A.; Tognoni, G.; Cohn, J. N. Direct Comparison of B-Type Natriuretic Peptide (BNP) and Amino-Terminal ProBNP in a Large Population of Patients with Chronic and Symptomatic Heart Failure: The Valsartan Heart Failure (Val-HeFT) Data. *Clin. Chem.* **2006**, *52*, 1528−1538.

(5) Januzzi, J. L.; Troughton, R. Are Serial BNP Measurements Useful in Heart Failure Management? *Circulation* **2013**, *127*, 500−508.

(6) Pollok, N. E.; Rabin, C.; Walgama, C. T.; Smith, L.; Richards, I.; Crooks, R. M. Electrochemical Detection of NT-ProBNP Using a Metalloimmunoassay on a Paper Electrode Platform. *ACS Sens.* **2020**, *5*, 853−860.

(7) Cai, H.; Zhu, N.; Jiang, Y.; He, P.; Fang, Y. Cu@Au Alloy Nanoparticle as Oligonucleotides Labels for Electrochemical Stripping Detection of DNA Hybridization. *Biosens. Bioelectron.* **2003**, *18*, 1311−1319.

(8) Oezaslan, M.; Hasché, F.; Strasser, P. PtCu3, PtCu and Pt3Cu Alloy Nanoparticle Electrocatalysts for Oxygen Reduction Reaction in Alkaline and Acidic Media. *J. Electrochem. Soc.* **2012**, *159*, B444−B454.

(9) Peretyazhko, T. S.; Zhang, Q.; Colvin, V. L. Size-Controlled Dissolution of Silver Nanoparticles at Neutral and Acidic PH Conditions: Kinetics and Size Changes. *Environ. Sci. Technol.* **2014**, *48*, 11954−11961.

(10) Hasan, S. A Review on Nanoparticles: Their Synthesis and Types. *Res. J. Recent Sci.* **2014**, *4*, 1−3.

(11) Ma, D.; Hugener, T. A.; Siegel, R. W.; Christerson, A.; Mårtensson, E.; Önneby, C.; Schadler, L. S. Influence of Nanoparticle Surface Modification on the Electrical Behaviour of Polyethylene Nanocomposites. *Nanotechnology* **2005**, *16*, 724−731.

(12) Hong, R.; Pan, T.; Qian, J.; Li, H. Synthesis and Surface Modification of ZnO Nanoparticles. *Chem. Eng. J.* **2006**, *119*, 71−81.

(13) Bagwe, R. P.; Hilliard, L. R.; Tan, W. Surface Modification of Silica Nanoparticles to Reduce Aggregation and Nonspecific Binding. *Langmuir* **2006**, *22*, 4357−4362.

(14) DeGregory, P. R.; Tapia, J.; Wong, T.; Villa, J.; Richards, I.; Crooks, R. M. Managing Heart Failure at Home with Point-of-Care Diagnostics. *IEEE J. Transl. Eng. Heal. Med.* **2017**, *5*, 2800206.

(15) Qin, X.; Liu, L.; Xu, A.; Wang, L.; Tan, Y.; Chen, C.; Xie, Q. Ultrasensitive Immunoassay of Proteins Based on Gold Label/Silver Staining, Galvanic Replacement Reaction Enlargement, and in Situ Microliter-Droplet Anodic Stripping Voltammetry. *J. Phys. Chem. C* **2016**, *120*, 2855−2865.

(16) Joshi, P. P.; Yoon, S. J.; Hardin, W. G.; Emelianov, S.; Sokolov, K. V. Conjugation of Antibodies to Gold Nanorods through Fc Portion: Synthesis and Molecular Specific Imaging. *Bioconjugate Chem.* **2013**, *24*, 878−888.

(17) Lee, K. M.; Neogi, A.; Basu Neogi, P.; Kim, M.; Kim, B.; Luchowski, R.; Gryczynski, Z.; Calander, N.; Choi, T. Y. Silver Nanostructure Sensing Platform for Maximum-Contrast Fluorescence Cell Imaging. *J. Biomed. Opt.* **2011**, *16*, 056008.

(18) Hu, T.; Chen, C.; Huang, G.; Yang, X. Antibody modified-silver nanoparticles for colorimetric immuno sensing of A$\beta$(1-40/1-42) based on the interaction between $\beta$-amyloid and Cu2+. *Sens. Actuators, B* **2016**, *234*, 63−69.

(19) Rekha, C. R.; Nayar, V. U.; Gopchandran, K. G. Synthesis of Highly Stable Silver Nanorods and Their Application as SERS Substrates. *J. Sci.: Adv. Mater. Devices* **2018**, *3*, 196−205.

(20) Katz, E.; Willner, I.; Wang, J. Electroanalytical and Bioelectroanalytical Systems Based on Metal and Semiconductor Nanoparticles. *Electroanalysis* **2004**, *16*, 19−44.

(21) Cunningham, J. C.; Scida, K.; Kogan, M. R.; Wang, B.; Ellington, A. D.; Crooks, R. M. Paper Diagnostic Device for Quantitative Electrochemical Detection of Ricin at Picomolar Levels. *Lab Chip* **2015**, *15*, 3707−3715.

(22) DeGregory, P. R.; Tsai, Y.-J.; Scida, K.; Richards, I.; Crooks, R. M. Quantitative Electrochemical Metalloimmunoassay for TFF3 in Urine Using a Paper Analytical Device. *Analyst* **2016**, *141*, 1734−1744.

(23) Mohammed, M.-I.; Desmulliez, M. P. Y. Lab-on-a-Chip Based Immunosensor Principles and Technologies for the Detection of Cardiac Biomarkers: A Review. *Lab Chip* **2011**, *11*, 569−595.

(24) Mainville, C. A.; Clark, G. H.; Esty, K. J.; Foster, W. M.; Hanscom, J. L.; Hebert, K. J.; Lyons, H. R. Analytical validation of an immunoassay for the quantification of N-terminal pro-B-type natriuretic peptide in feline blood. *J. Vet. Diagn. Invest.* **2015**, *27*, 414−421.
(25) Li, H.; Yin, X.; Sun, D.; Xia, K.; Kang, C.; Chu, S.; Zhang, P.; Wang, H.; Qiu, Y. Detection of NT-pro BNP Using Fluorescent Protein Modified by Streptavidin as a Label in Immunochromatographic Assay. *Sens. Bio-Sens. Res.* **2016**, *11*, 1−7.
(26) Hwang, P.; Guyda, H.; Friesen, H. A Radioimmunoassay for Human Prolactin. *Proc. Natl. Acad. Sci. U.S.A.* **1971**, *68*, 1902−1906.
(27) Kim, D.; Daniel, W. L.; Mirkin, C. A. Microarray-Based Multiplexed Scanometric Immunoassay for Protein Cancer Markers Using Gold Nanoparticle Probes. *Anal. Chem.* **2009**, *81*, 9183−9187.
(28) Liu, X.; Dai, Q.; Austin, L.; Coutts, J.; Knowles, G.; Zou, J.; Chen, H.; Huo, Q. A One-Step Homogeneous Immunoassay for Cancer Biomarker Detection Using Gold Nanoparticle Probes Coupled with Dynamic Light Scattering. *J. Am. Chem. Soc.* **2008**, *130*, 2780−2782.
(29) Hainfeld, J. F.; Furuya, F. R. A 1.4-Nm Gold Cluster Covalently Attached to Antibodies Improves Immunolabeling. *J. Histochem. Cytochem.* **1992**, *40*, 177−184.
(30) Cheng, L.; Zhu, G.; Liu, G.; Zhu, L. FDTD Simulation of the Optical Properties for Gold Nanoparticles. *Mater. Res. Express* **2020**, *7*, 125009.
(31) Simon, J.; Udayan, S.; Bindiya, E. S.; Bhat, S. G.; Nampoori, V. P. N.; Kailasnath, M. Optical Characterization and Tunable Antibacterial Properties of Gold Nanoparticles with Common Proteins. *Anal. Biochem.* **2021**, *612*, 113975.
(32) Boisselier, E.; Astruc, D. Gold Nanoparticles in Nanomedicine: Preparations, Imaging, Diagnostics, Therapies and Toxicity. *Chem. Soc. Rev.* **2009**, *38*, 1759−1782.
(33) Cunningham, J. C.; Kogan, M. R.; Tsai, Y.-J.; Luo, L.; Richards, I.; Crooks, R. M. Paper-Based Sensor for Electrochemical Detection of Silver Nanoparticle Labels by Galvanic Exchange. *ACS Sens.* **2016**, *1*, 40−47.
(34) Bard, A. J.; Faulkner, L. R. *Electrochemical Methods: Fundamentals and Applications*; Harris, D., Swain, E., Robey, C., Aiello, E., Eds.; 2nd ed.; John Wiley & Sons, Inc.: Hoboken, 2001.
(35) González, E.; Arbiol, J.; Puntes, V. F. Carving at the Nanoscale: Sequential Galvanic Exchange and Kirkendall Growth at Room Temperature. *Science* **2014**, *1377*, 1377−1381.
(36) Wiley, B.; Sun, Y.; Chen, J.; Cang, H.; Li, Z.-Y.; Li, X.; Xia, Y. Shape-Controlled Synthesis of Silver and Gold Nanostructures. *MRS Bull.* **2005**, *30*, 356−361.
(37) Peng, Y.; Rabin, C.; Walgama, C. T.; Pollok, N. E.; Smith, L.; Richards, I.; Crooks, R. M. Silver Nanocubes as Electrochemical Labels for Bioassays. *ACS Sens.* **2021**, *6*, 1111−1119.
(38) Tetin, S. Y.; Ruan, Q.; Saldana, S. C.; Pope, M. R.; Chen, Y.; Wu, H.; Pinkus, M. S.; Jiang, J.; Richardson, P. L. Interactions of Two Monoclonal Antibodies with BNP: High Resolution Epitope Mapping Using Fluorescence Correlation Spectroscopy. *Biochemistry* **2006**, *45*, 14155−14165.
(39) Skrabalak, S. E.; Au, L.; Li, X.; Xia, Y. Facile Synthesis of Ag Nanocubes and Au Nanocages. *Nat. Protoc.* **2007**, *2*, 2182−2190.
(40) Au, L.; Lu, X.; Xia, Y. A Comparative Study of Galvanic Replacement Reactions Involving Ag Nanocubes and AuCl2−or AuCl4−. *Adv. Mater.* **2008**, *20*, 2517−2522.
(41) Lu, X.; Au, L.; McLellan, J.; Li, Z.-Y.; Marquez, M.; Xia, Y. Fabrication of Cubic Nanocages and Nanoframes by Dealloying Au/Ag Alloy Nanoboxes with an Aqueous Etchant Based on Fe(NO3)3 or NH4OH. *Nano Lett.* **2007**, *7*, 1764−1769.
(42) Sun, Y.; Mayers, B. T.; Xia, Y. Template-Engaged Replacement Reaction: A One-Step Approach to the Large-Scale Synthesis of Metal Nanostructures with Hollow Interiors. *Nano Lett.* **2002**, *2*, 481−485.
(43) Chen, J.; Mclellan, J. M.; Siekkinen, A.; Xiong, Y.; Li, Z.-Y.; Xia, Y. Facile Synthesis of Gold−Silver Nanocages with Controllable Pores on the Surface. *J. Am. Chem. Soc.* **2006**, *128*, 14776−14777.
(44) Pollok, N. E.; Rabin, C.; Smith, L.; Crooks, R. M. Orientation-Controlled Bioconjugation of Antibodies to Silver Nanoparticles. *Bioconjugate Chem.* **2019**, *30*, 3078−3086.
(45) Thermo Fisher. *Dynabeads MyOne Streptavidin T1 Protocol*; 2016.
(46) Bio-Rad Laboratories. *LYNX Rapid Plus Biotin (Type 2) Antibody Conjugation Kit Protocol*, 2011, 2−4.


https://doi.org/10.1021/acsanm.1c02207
*ACS Appl. Nano Mater.* 2021, 4, 10764−10770